Using Raw Star Signals in the Monitoring of GOES Imager Visible–Channel Responsivities

I-Lok Chang[a,b] Charles Dean[b] Michael Weinreb[c] Xiangqian Wu[d]

Dejiang Han[e] Kenneth Mitchell[e] Zhenping Li[f] Gordana Sindic–Rancic[g] Fanfang Yu[h]

[a]American University, 4400 Massachusetts Avenue, NW, Washington, D.C., 20016, USA;
[b]Perot Systems Corporation, 4500 Forbes Boulevard Suite 200, Lanham, MD, 20706, USA
[c]Riverside Technology, Inc., NOAA/NESDIS/OSD, NSOF, Room 1378, 4231 Suitland Road, Suitland, MD, 20746, USA
[d]NOAA/NESDIS/ORA,E/RA2, 5200 Auth Road, Camp Springs, MD, 20745-4304,USA
[e]ASRC Aerospace Corporation, 6303 Ivy Lane, Suite 800, Greenbelt, MD, 20707, USA
[f]SGT, Inc., 7701 Greenbelt Road, Suite 400, Greenbelt, MD, 20770, USA
[g]IMSG, 5200 Auth Road, Camp Springs, MD, 20746, USA
[h]ERT, Inc., NOAA/NESDIS/STAR(ORA), 5200 Auth Road, Camp Springs, MD, 20745, USA

ABSTRACT

Stars are regularly observed in the visible channels of the GOES Imagers for real-time navigation operations. However, we have been also using star observations off-line to deduce the rate of degradation of the responsivity of the visible channels. We estimate degradation rates from the time series of the intensities of the Imagers' output signals when viewing stars, available in the GOES Orbit and Attitude Tracking System (OATS). We begin by showing our latest results in monitoring the responsivities of the visible channels of the Imagers on GOES–8, –9, –10, –11 and –12. Unfortunately, the OATS computes the intensities of the star signals with approximations suitable for navigation, not for estimating accurate signal strengths, and thus we had to develop objective criteria for screening out unsuitable data. With several layers of screening, our most recent trending method yields smoother time series of star signals, but the time series are populated by a smaller pool of stars. With the goal of simplifying the task of data selection and to retrieve stars that have been rejected in the screening, we tested a technique that accessed the raw star measurements before they were processed by the OATS. We developed formulations that not only produced star signals more suitable for monitoring the changes in the Imager's outputs from views of constant-irradiance stellar sources, but also gave more information on the radiometric characteristics of the visible channels. We present specifics of this technique together with sample results. We discuss improvements in the quality of the time series that allow for more reliable inferences on the gradually changing responsivities of the visible channels. We describe further contributions of this method to monitoring of other performance characteristics of the visible channel of an Imager.

Keywords: Calibration, visible, GOES, stars, time series

Further author information: (Send correspondence to I-Lok Chang)
I-Lok Chang: E-mail: ilchang@american.edu, Telephone: (202)885-3132, Fax: (202)885-3155
Charles Dean: E-mail: charlie.dean@noaa.gov, Telephone: (301)928-5282
Michael Weinreb: E-mail: michael.weinreb@noaa.gov, Telephone: (301)817-4609, Fax: (301)817-4403
Xiangqian Wu: E-mail: Xiangqian.Wu@noaa.gov, Telephone: (301)763-8136 ext 138, Fax: (301)763-8580
Dejiang Han: E-mail Dejiang.Han@noaa.gov, Telephone: (301)817-4119, Fax: (301)457-5713
Kenneth Mitchell: kenneth.j.mitchell@noaa.gov, Telephone: (301)817-4194
Zhenping Li: Zhenping.Li@noaa.gov, Telephone: (301)817-4217
Gordana Sindic–Rancic: E-mail: gordana.s.rancic@noaa.gov, Telephone: (301)763-8999, Fax: (301)763-8580
Fangfang Yu: E-mail: Fangfang.Yu@noaa.gov, Telephone: (301)763-8207 ext 182

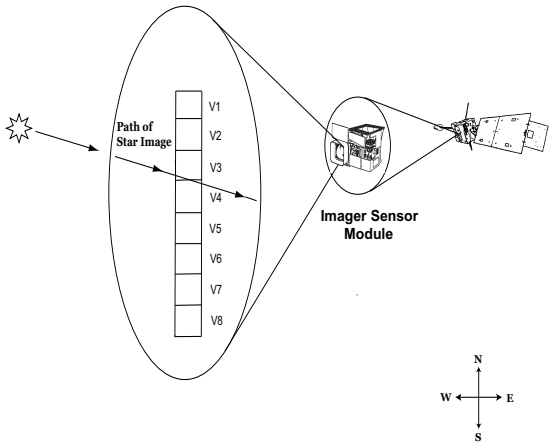

Figure 1. The eight detectors of the visible channel of an Imager conducting a star look.

1. INTRODUCTION

The National Oceanic and Atmospheric Administration (NOAA) commenced its management and operation of the series of Geostationary Environmental Satellites (GOES) in 1975, with the launch of GOES–A in October of 1975. Currently there are three GOES satellites in daily operation, GOES-10, -11 and -12. Each satellite observes the Earth and its atmosphere by acquiring images and radiometric data through two instruments, the Imager and the Sounder. The Imager is a radiometer with four channels in the thermal infrared and one in the visible part of the spectrum. There is no on-board calibration facility for the visible channel of the Imager, as the channel was originally not intended for quantitative use. If the responsivity in the visible channel were known to vary only slightly within time, this would not be an important deficiency, but it is known that, in fact, the responsivities of the visible channels of all GOES Imagers are declining at rate of a few percent per year. Because of that, and because the user community is increasingly using data in the visible channel for quantitative applications, we have recognized the need for monitoring quantitatively the responsivity of the visible channel. Such work is now an ongoing effort at the National Environmental Satellite Data and Information (NESDIS) of NOAA. This paper is a continuation report on advances of a vicarious calibration technique that has been in use for almost ten years. The basis of the technique is described by Bremer, et al.[1] (1998), which used observations of stars processed by the navigation system to monitor changes in the responsivity of the Imager's visible channel. We call this technique Method 1. This procedure has been improved and has evolved into a Method 2. Then we departed from Method 2 and essentially started over from the raw data to develop a more self-consistent and flexible procedure, which we call Method 3. In this paper, we give star monitoring results using the three methods, with star data spanning the period 1995–2008, and with observations from the Imagers aboard the satellites GOES–8, –9, –10, –11 and -12. In Chang, et al.[2,3], the first two methods have been presented in detail. For completeness we give here a summary description of the two methods. At this time, the collection of daily data for Method 3 is under way. The data is providing a range of information for refining the method, providing useful error bounds, and enabling us to make further inferences on certain physical characteristics of a visible channel. We discuss progress in this direction in Section 4 of this paper.

2. STAR–BASED CALIBRATION USING SIGNALS COMPUTED FOR SATELLITE NAVIGATIONAL OPERATIONS

Many stars are light sources with stable and well-quantified intensities. The Imager of a GOES satellite observes stars at regular time intervals as a part of the operational process for determining the Imager's orbit and attitude. The intensity of the star light, in arbitrary units, is also measured and archived. Figure 1 illustrates the crossing of a star image over the detectors of a visible channel in a star sensing operation. The visible channel is equipped with a linear array of eight detectors oriented essentially in the north–south direction. In Figure 2, the two plots show the intensity of the star light

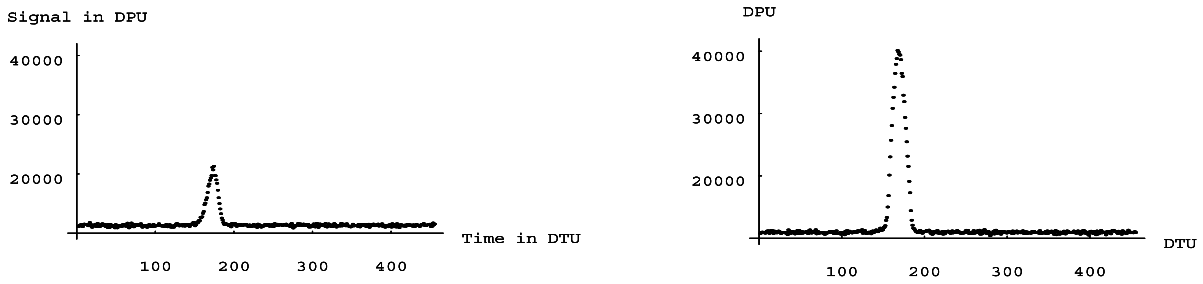

Figure 2. Measurements received from Detector 3 (left) and Detector 4 (right) of the visible channel of the Imager of GOES–12, in a star look of α–Aql, conducted on November 4, 2004. One Detector Time Unit (one DTU) is 400/21840 second. One Detector Pixel Unit (one DPU) is one count in a pixel value.

measured by Detector 3 and Detector 4 as each detector registered the crossing of a portion of the star image. The data shown are actually a running sum of 400 individual samples from the detector. The individual samples are received at 21,800 pixels per second. The units on the abscissa are Detector Time Units (DTU), where one DTU is 400/21800 second. The units on the ordinate are Detector Pixel Units (DPU), where one DPU is a one (digital) count output (after summing over the 400 samples) of the channel.

The measurements such as those shown in Figure 2 are transmitted to the ground and processed in real time in the Sensor Processing System (SPS) computer at the Wallops Command and Data Acquisition Station. The SPS routinely generates, in real time, a set of statistics for each star sense. The statistics are then relayed to the GOES Orbit and Attitude Tracking System (OATS) at the Satellite Operations and Control Center in Suitland, MD, where computations based on the statistics are conducted to support navigation operations. At the OATS, an estimate of the intensity of the star image is made and archived in a database. This intensity is called the snr (signal–to–noise ratio) associated with the star image and is dimensionless. In a star sense operation, a sequence of looks at the same star may be executed. The composite snr for this star sense is the sum of all the star snr's from the looks where the star was detected. The estimation formula for the snr of a star look is a statistically based formula that involves two steps. First an estimate for the maximum height of the signal profile is made for each detector that detected a star crossing. Call this maximum height MI_i where i is the detector index. Then the snr associated with this star look is a sum of the form $\sum \mathrm{W}_i\ \mathrm{MI}_i$, summing over all the detectors where a part of the star image has crossed. The constant W_i is a detector-dependent factor of the form W = Relative Gain/Noise. Thus if a star image crossed over only one detector, the snr of this star look is simply an estimated maximum intensity scaled with a Relative Gain/Noise factor.

We use the star snr's produced by the OATS as described in the previous paragraph to provide a time series that over a sufficiently long term shows a gradual decrease that reflects the degradation in the responsivity of a visible channel. Figure 3 shows such time series of the star β–Cnc from GOES–12. Time series from GOES–8, –10 and –11 constructed using Method 1 have very similar appearances. For each satellite GOES–8, –9, –10, –11 and –12, we choose a collection of stars that are sufficiently bright and have been observed with relatively high frequencies. The time series of each star is fitted with an exponential function of the form Be^{-At}, where t is the number of days since the launch of the satellite. The coefficient A is called a degradation rate. Usually we expressed this rate as an annual rate, where annual rate = $(365 \times A)\%$. Table 1 shows the average degradation rate for each satellite, where the average rate is determined from the time series of the stars chosen for the satellite. This method is the one introduced in Bremer, et al[1](1998). This is Method 1.

The main reason for using the name Method 1 is that we have over time found improvements for this method as we gained more understanding of the star sensing process and the computational steps employed at the OATS to derive the star snr's. The improved method is called Method 2. We nevertheless retain Method 1 and publish its estimates to maintain continuity in the reported calibration results.

In Method 2, we incorporated additional steps into Method 1 to remove several types of data that may contain significant inaccuracies. Observe that in Figure 3, the time series has a band of points with high values, above the main part of the series in the middle. There is also a band of points with low values, below the middle band. Many signals in the high band are results of summing the weighted maximum intensity MI_i over several detectors, and over several star looks if star signals were found in more than one star look. Such a summing process can be an over estimate of the actual intensity of the star signal. For this reason, we remove all star data obtained from star senses that involved more than one detector, and also the star senses where a star was detected in more than one look.

For the low data points, many such points occurred when a star image crossed over a detector at the top or bottom of the linear array of detectors – crossing over detector 1 or detector 8. After observing numerous low signals occurring in such crossings, we conclude that a low signal must be the result of having only a part of the star image falling on an edge detector. We therefore exclude all star data that involve crossing over detector 1 or detector 8.

The data that remain are therefore star signals of single-detector crossing, occurring on one of the interior detectors. Most of the data in this group fall on the middle band, given by only one term, $\mathrm{W}_i\mathrm{MI}_i$. We found that by removing the unnecessary scaling factors W_i, which are different for each detector, the points in this band cluster significantly closer, with a smaller vertical scatter. Figures 4, 5 and 6 are obtained by applying the three types of data selection to the data that are used in Method 1. (Here the units on the ordinate are DPU, but the values are smaller than those in Figure 2 because the signals have been divided by 400. Note, also, that these units are also different from those of Figure 3, which are the OATS–produced snr's [dimensionless]). We call this improved procedure Method 2.

For GOES–8, –10, –11 and –12, by applying Method 2 to the star data that gave the degradation coefficients of Table 1, we obtained the degradation coefficients in Table 2. In both tables, it is apparent that standard error of the mean degradation rates (over the approximately 40 stars included) varies among the Imagers on the different satellites, and is by far the largest for GOES–11. We do not understand the reason for this variation.

3. COMPUTING A STAR SIGNAL DIRECTLY FROM THE DETECTOR MEASUREMENTS: METHOD 3

The time series of star signals generated with Method 2 have been providing stable estimates of the exponential degradation rates of the series. Applying this method to construct time series, however, requires intricate filtering and correction of the OATS star data, and constant vigilance on changes in the databases of the OATS that may affect the accuracies of the computed star snr's. Furthermore, many strong star signals from brighter stars cannot be obtained through Method 2, because an image of a bright star often spans more than one detector, and such signals are excluded from the time series. (Although the image of a dimmer star presumably has the same spatial distribution, its wings more quickly become insignificant relative to the noise in the channel.) The need to maintain updates on changes at the OATS related to the calculation of the snr's was a primary reason that motivated us to look for ways to determine star signals with only minimal dependence on the data processing at the OATS. We have developed such a method, called Method 3. This method has the additional advantage that signals of brighter stars are now included in the time series.

We found that in the flow of star data from an Imager to the OATS, there is one stage between the SPS and the OATS where we could access the signal stream and make a copy of the measurements of each star look. The data at this stage is of the form shown on Figure 2, where the measurements of a star look consist of the initial eight profiles whose points are intensity counts registered at equally spaced time marks. In Method 3, we compute a star signal from this set of profiles. Specifically, for each (detector) profile that contains star pixels, we first shift the profile to a base (zero signal) and scale the resulting profile with a factor of $1/400$ (to account for the fact that the signal is actually the sum over 400 individual samples: see Chang, et al.[3]). For the numerical value of the base level we use the median of the data points in the profile. The median filter is effective as long as the star-crossing feature is narrow relative to the full extent of the profile, as it is in Figure 2. Next we compute the complete signal profile by adding all the profiles from detectors that registered a star crossing. The addition is done in a time-coherent (point-by-point) manner. Finally we compute a peak

Table 1. Estimated degradation rates from Method 1. Each estimated rate $\hat{A}$ is the average of the A-coefficients of approximately 40 stars. The stated error is the usual standard error of the mean.

Spacecraft	$\hat{A}$(annual rate)	Length of Time Series
GOES–8	$4.96 \pm 0.09\%$	April 10, 1995 to April 1, 2003
GOES–9	$5.41 \pm 0.28\%$	August 7, 1995 to May 16, 1998
GOES–10	$4.69 \pm 0.07\%$	March 21, 1998 to May 22, 2008
GOES–11	$3.92 \pm 0.70\%$	June 21, 2006 to May 22, 2008
GOES–12	$4.25 \pm 0.10\%$	April 1, 2003 to May 22, 2008

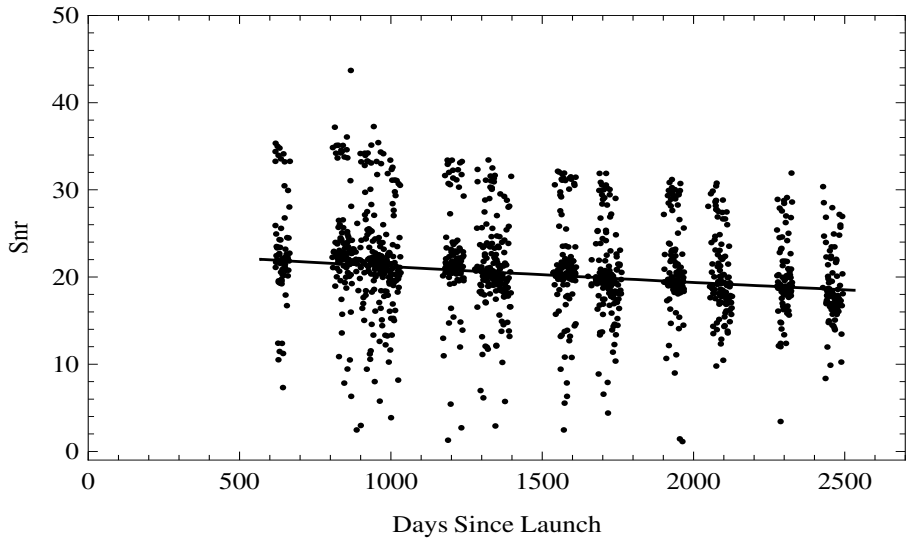

Figure 3. A time series of star signals of β-Cnc from GOES–12. The data selection method is Method 1. The method is applied to data obtained over the period April 1, 2003, to May 22, 2008. Day 1 is the launch date of GOES–12: July 23, 2001.

Table 2. Estimated degradation rates using Method 2. Each estimated rate $\hat{A}$ is the average of the A-coefficients of approximately 60 stars. The stated error is the usual standard error of the mean.

Spacecraft	$\hat{A}$(annual rate)	Length of Time Series
GOES–8	$4.86 \pm 0.08\%$	October 19, 1995 to April 1, 2003
GOES–10	$3.47 \pm 0.06\%$	January 4, 2001 to May 22, 2008
GOES–11	$5.55 \pm 0.47\%$	June 21, 2006 to May 22, 2008
GOES–12	$4.78 \pm 0.06\%$	April 1, 2003 to May 22, 2008

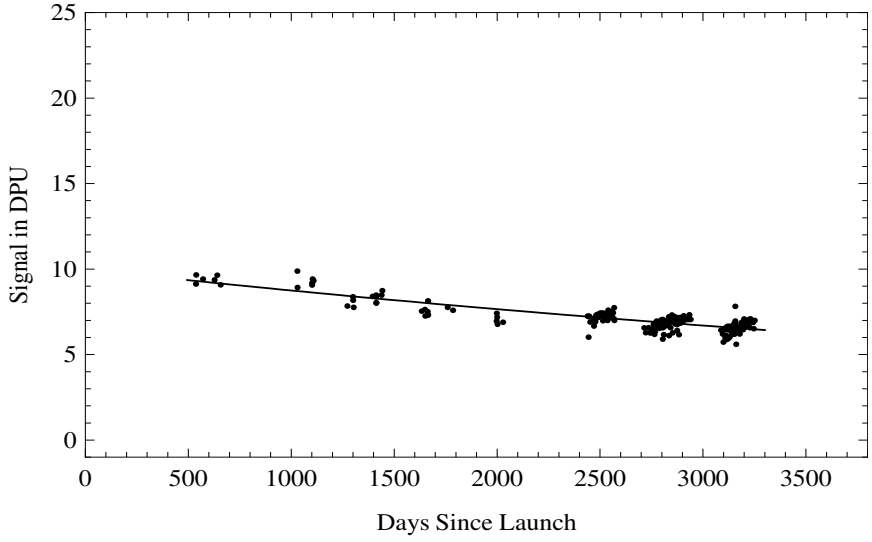

Figure 4. A time series of star signals of β-Cnc from GOES–8 and the exponential fit for this time series. The data selection method is Method 2. The method is applied to data obtained over the period October 1, 1995 to April 1, 2003. Day 1 is the launch date of GOES–8: April 13, 1994.

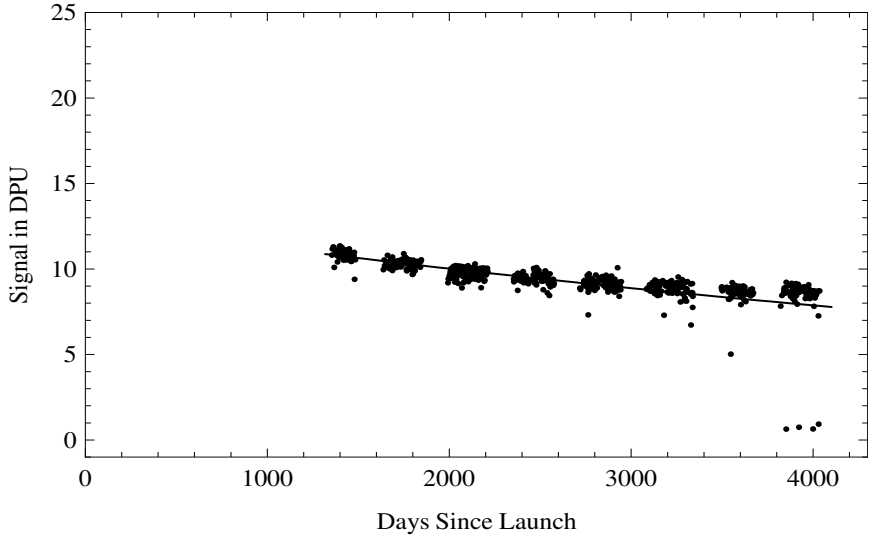

Figure 5. A time series of star signals of β-Cnc from GOES–10 and the exponential fit for this time series. The data selection method is Method 2. The method is applied to data obtained over the period January 7, 2001, to May 22, 2008. Day 1 is the launch date of GOES–10: April 25, 1997.

signal from this composite profile as the highest average value of k consecutive points. Currently k is chosen to be 8. This maximum average value is the star signal for this star look. Figure 7 is the composite profile derived from the star look shown on Figure 2. The selection rule of rejecting star crossings in detector 1 and detector 8 remains in force in this method.

We started to collect data for Method 3 in October of 2004. The complete set of data, however, is still quite sparse because the data collection, not yet automated until recently, usually occurred one day a week. In April of 2008, we automated such a data collection into a daily activity.

We have been using the available data to conduct tests on the algorithm of Method 3. One of our first tests was to superimpose the time series of a star using Method 3 over the time series of the same star and the same satellite using Method 2. In Chang, et al.[3], we discuss reasons why the two time series should almost coincide. At this time, we are finding such congruence in the many cases we have examined. In Figure 8, the time series of Method 2 is marked with dots, and the time series of Method 3 is marked with circles. Except for a very few points, they appear to be similar.

For the time series of Figure 8, with the points A and B excluded via two new objective data–selection rules (explained in the next section), the degradation rate of the time series of Method 3 changes from 3.4%/yr to 4.9%/yr. The degradation rate of the time series of Method 2 in this case is estimated to be 4.4%/yr.

Table 3 contains average degradation rates for GOES–10 and –12 derived from time series computed with Method 3. With the addition of the two data–selection rules we shall describe below, Method 3 has been providing time series that have shown good coincidence with the corresponding time series computed using Method 2, despite the relatively sparse amount of data we are able to compile with only once-a-week collections. We also expect the degradation rates estimated from Method 3 will be more stable because the method avoids some irrelevant and possibly incorrect operations in the computational algorithms of the OATS that we could not remove in Methods 1 and 2. Because of the similarity between the results of Methods 2 and 3 shown in Tables 2 and 3, respectively, we have good confidence on the potential of Method 3.

4. ADDITIONAL BENEFITS FROM USE OF THE DIRECT DETECTOR STAR SIGNALS

Data of Method 3 contain information that we have not been able to deduce from the data of Method 1 and Method 2, because such information has been filtered out at various stages of processing. The new information has been providing further understanding of the nature of the measurement process in a visible channel and allows us to enhance various calibration procedures. We describe here three such cases. The first case concerns certain physical states within an Imager module. The second and the third are on the enhancement of data selection and analysis procedures aided by such information.

On the time series of many stars, we have observed with Method 2 a saw-tooth type of annual cycle where each annual segment of a star time series exhibits a time dependence that is not congruent with the long-term degradation effect. For GOES–8, the annual segments tend to slope upward, while for GOES–12, the movement is mostly downward – see Figures 4 and 6, respectively. A star time series of GOES-10, however, has far less observable variation in such manner, as we see in Figure 5. Recall that the gap between any two segments is the result of removing star signals that were measured within five hours on each side of a local midnight, which we term the "exclusion period" (see Chang, et al.[2,3]). To examine how such cycles move continuously in time we plot in Figure 9 a complete time series that includes the star signals that have been excluded in Figure 6. We see a variation in the star signals fluctuating from the normal level outside the exclusion period to very low values within the exclusion period, and then quite rapidly returning to the normal level. From the raw data, we find some correlation of such signal variation with the variation in the shape of the individual signal profiles measured on the eight detectors. In Figure 10 we regard a profile of the normal type: a Gaussian-type signal profile that is reasonably symmetric. In Figure 11 we see profiles of the same star that show deformations such as concavities and sometimes with certain amount of widening at the base of the Gaussian portion . Such deformation almost always is accompanied by a decrease in the measured star signal. Such decrease in signal can be of the magnitude of as large as 40% of the normal signal. We observed that the deformation of the profiles occur more frequently and more severely in the exclusion periods.

By studying the change in the shapes of the profiles, we surmise that the fluctuation in the star light in the annual cycle described above is likely a result of changes in the focusing properties of the Imager, likely a result of thermally-driven expansions and contractions within the optical train of the Imager. The changes are most likely induced by the variation of the temperature distribution within the Imager instrument as the angle between the sun and the satellite changes. Such changes can explain all three apparently different annual cycles seen in GOES–8, –10, and –12. We are formulating some numerical parameters to reflect the presence of such annual variation in a star time series. One such model that has been quite satisfactory is the use of a function of the form $f(t) = Be^{-At}(m[t]t + b[t])$, where A is the overall degradation rate and $m[t]t + b[t]$ is a linear function on each segment of the time series. Such a formulation apparently is necessary for a good fit to the time series of Method 2. However, preliminary evidence indicates that the annual effects seen for Method 2 in Figures 4 –6 do not occur, or occur with a much lower amplitude, within the time series of Method 3. Thus a highly precise model such as that described here may not bring any substantial improvement in the accuracy of our estimated degradation rates for the visible channels.

Another advantage of having data of Method 3 is that, because it requires access to the raw data, it provides more quantitative information on the uncertainties in the star signal. We find that the pixels of a detector signal profile that contains no star event show a histogram distribution very much in the shape of a normal (Gaussian) density function, with an estimated standard deviation of the size of 0.45 (in DPU) that remains quite constant from satellite to satellite. Furthermore, the maximum and the minimum pixel signals of such background signals are mostly between -2.0 and 2.0 DPU. AS we apply some statistical tests to such signals, we find that the sum of several such signal profiles exhibit the characteristics of the sum of Gaussian variables which are identically distributed and stochastically independent. This knowledge is useful in estimating the uncertainty in the computed degradation rates, under the assumption that the background signals constitute the dominant (additive) components of the noise in the measured star signals.

One further consequence of analyzing the raw data for Method 3 is that additional data selection rules can be formulated as we are now capable of studying details of other anomalous occurrences in the time series of star signals. In Figure 8, two points from Method 3 have fallen conspicuously outside the region of coincidence with the time series of Method 2. We found that the relatively high point A occurred at a period of active solar flares (January 15–20, 2005). We have little doubt that something from the solar flares caused the significant increase in some measurements on Detector 2. The star profile that yielded the point A is displayed in the left chart of Figure 12. A high point occurred in the peak region of the star profile. The computed star signal using Method 3 in this case is 10.1 DPU, whereas the usual signal level of this star from January to March of 2005 is about 9.1 DPU. On another time series, the solar-flare activities of January 15–20 of 2005 no doubt had created a phantom star shown in the right-hand chart in Figure 12, where about seven data points somewhat above the base level had caused the SPS and OATS algorithms to interpret them as signals from the star ϵ-Eri. The computed star signal in this case is 1.9 DPU, whereas the usual star-signal level of this star during this period is about 6.0 DPU. In Method 3, we shall therefore exclude star measurements taken during days of high solar activity (using some published indices of NOAA on the levels of various solar activities).

The relatively low point B in Figure 8 is a star signal measured in the second of a sequence of two star looks on the same star, whose profiles are shown in Figure 13. In a star sense operation, within a time interval about 60 seconds, a sequence of several star looks can be conducted. For this example, the first look yielded a star signal of 6.79 DPU on Detector 1, whereas the second look yielded star signal of 0.70 DPU on Detector 3. We are working to explain how such disparate observations can be obtained for the same star in a sequential-look situation. In the meantime, we will exclude all sequential star-sensing events where one of the signals can deviate by more then 50% from the highest signal.

5. CONCLUSION

Star observations by GOES Imagers for determining orbit and attitude are providing stable information for monitoring the responsivities of the visible channels of the Imagers. Processing the star data *ab initio* in our Method 3, rather than post-processing the OATS product, allows improvements in precision and yield of the star signals, which we expect will lead to improvements in monitoring results. Furthermore, the unprocessed star signals for Method 3 have enabled us to

associate artifacts in the Imagers' star signals with optical effects within the Imager instruments.

ACKNOWLEDGMENTS

The authors are grateful to the NESDIS Office of Systems Development for funding via the GOES Improved Measurements and Product Assurance Plan (GIMPAP). The views, opinions, and findings contained in this paper are those of the authors and should not be construed as official National Oceanic and Atmospheric Administration or U. S. Government positions, policy, or decisions.

REFERENCES

1. Bremer, J.C., J. G. Baucom, H. Vu, M. P. Weinreb, and N. Pinkine, "Estimation of long-term throughput degradation of GOES 8 & 9 visible channels by statistical analysis of star measurements," in *Earth Observing Systems III*, *Proc. SPIE* **3439**, pp. 145–154, 1998.
2. Chang, I-L., D. Crosby, C. Dean, M. Weinreb, P. Baltimore, J. Baucom, D. Han, "Data selection criteria in star-based monitoring of GOES imager visible-channel responsivities," in *Imaging Spectrometry X*, *Proc. SPIE* **5546**, pp. 253–261, 2004.
3. Chang, I-L., D. Crosby, C. Dean, M. Weinreb, P. Baltimore, J. Baucom, D. Han, "Improvements in star-based monitoring of goes imager visible-channel responsivities," in *Earth Observing System X*, *Proc. SPIE* **5546**, pp. 58820M1–58820M11, 2005.

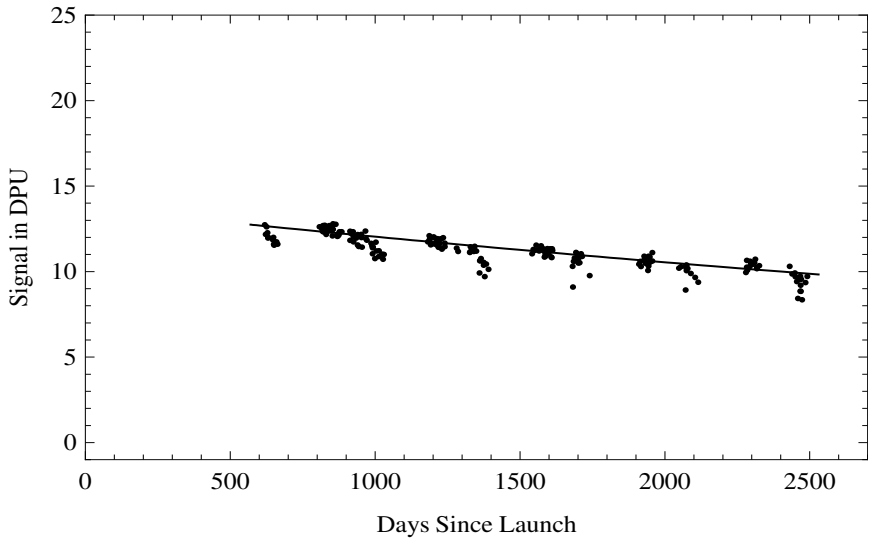

Figure 6. A time series of star signals of β-Cnc from GOES–12 and the exponential fit for this time series. The data selection method is Method 2. The method is applied to data obtained over the period April 2, 2003, to May 22, 2008. Day 1 is the launch date of GOES–12: July 23, 2001.

Table 3. Estimated degradation rates using Method 3. Each estimated rate $\hat{\text{A}}$ is the average of the A-coefficients of approximately 50 stars. The stated error is the usual standard error of the mean.

Spacecraft	**$\hat{\text{A}}$(annual rate)**	**Length of Time Series**
GOES–10	$2.35 \pm 0.35\%$	October 27, 2004 to May 22, 2008
GOES–12	$4.00 \pm 0.22\%$	October 27, 2004 to May 22, 2008

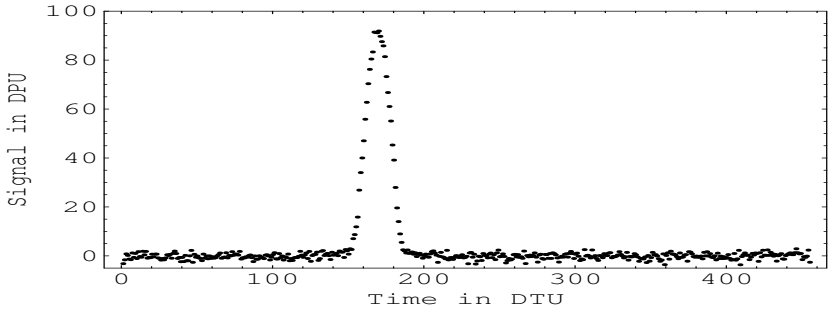

Figure 7. A Composite Profile computed for the star crossing of α–Aql in Figure 2. This profile (signal versus time) is obtained from the two individual profiles shown in Figure 2. The two individual profiles are first shifted to zero levels and then scaled with $1/400$, then summed to yield the composite profile.

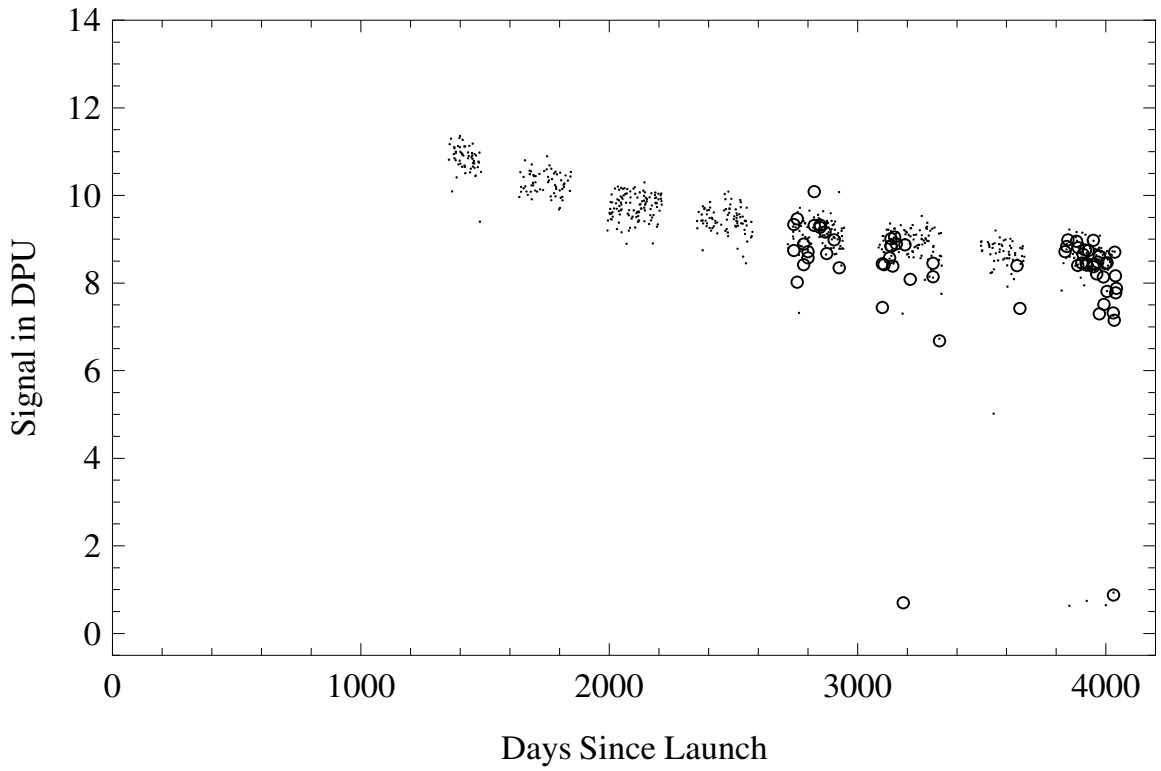

Figure 8. Comparison of a time series of the star β-Cnc computed using Method 2 and a time series of the same star computed using Method 3. The time series in dots: GOES–10, January 7, 2001 to April 1, 2007, Method 2. The time series in circles: GOES–10, October 27, 2004 to June 5, 2006, Method 3. Superposition of the two time series shows coherence, but also leads to further data selection rules in Method 3 – exclusion of Point A and Point B.

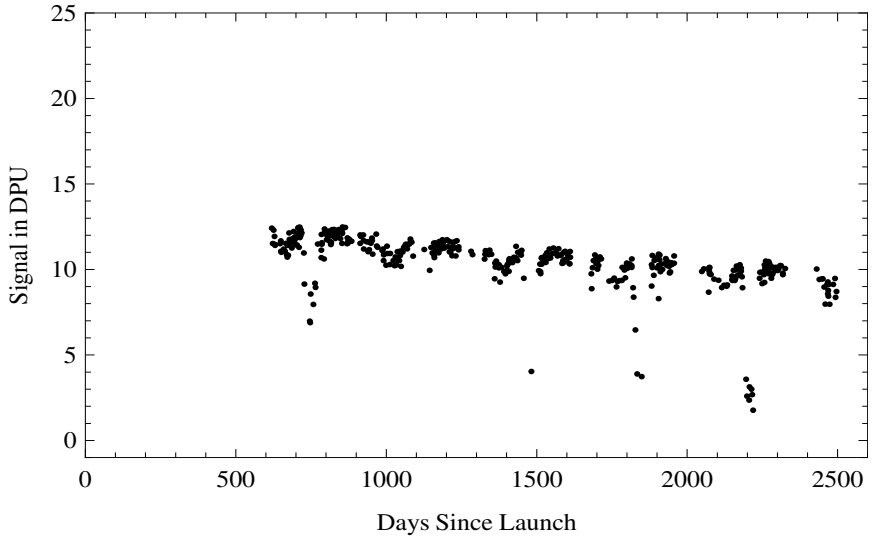

Figure 9. A time series of star signals of β-Cnc from GOES–12 without excluding star signals near local midnights. The data selection method is Method 2. The method is applied to data obtained over the period April 2, 2003, to May 22, 2008. Day 1 is the launch date of GOES–12: July 23, 2001.

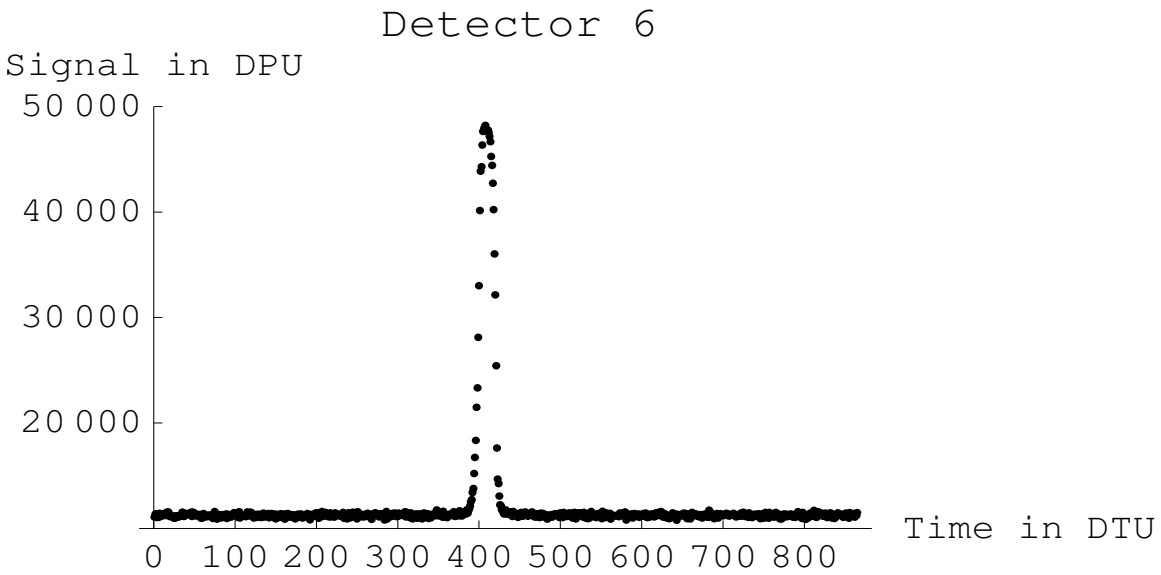

Figure 10. Signal profile of star α–Aql on Detector 5 of GOES–12, on April 19, 2005. The time is UTC 23:7:8.418. Local midnight is UTC 5:00:00. Detector 5 and Detector 7 also registered partial star crossings, but the values of the signals are too low to be shown. The total signal of this star look is 93.1 DPU.

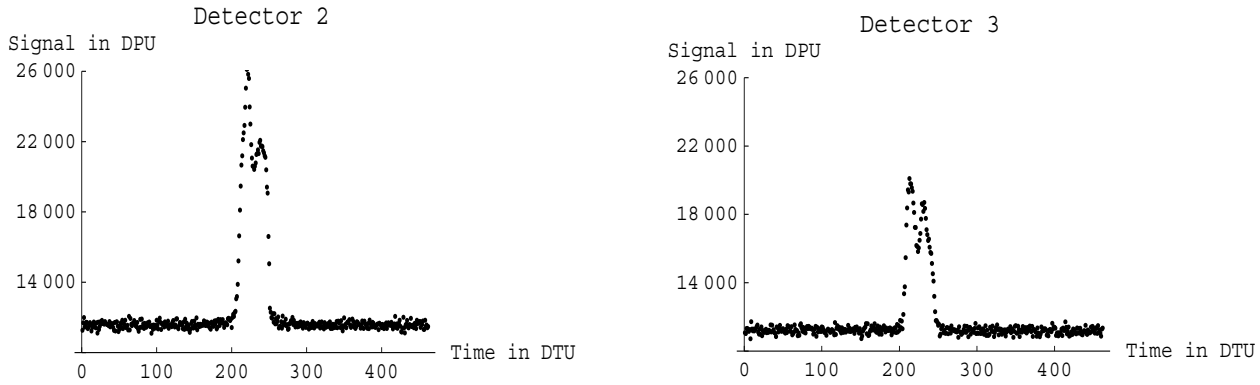

Figure 11. The image of star α–Aql spanned over Detector 2 and Detector 3 on GOES–12, on January 31, 2003. The time is UTC 4:27:1.942. Local midnight is UTC 5:00:00. Each signal profile shows deformations that usually indicate a loss in the signal strength . The total signal of this star look is 49.36 DPU.

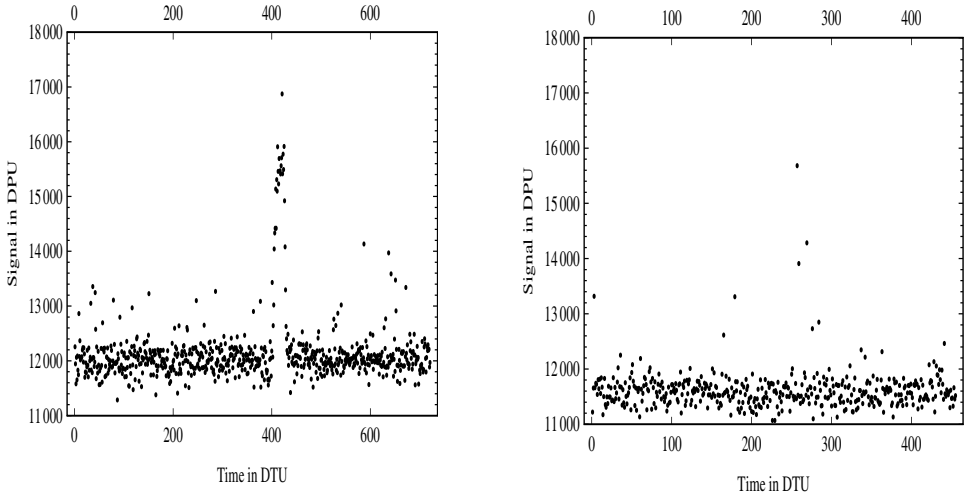

Figure 12. Anomalous star signals recorded during a period of intense solar flares, January 15 to 20, 2005: On the left is a star-signal profile of the star β-Cnc, recorded on January 17, 2005, from GOES–10, on Detector 2, with an unusually high point at the peak of the profile. On the right is a phantom star profile ascribed to the star ϵ–Eri, recorded on January 20, 2005, from GOES–10, on Detector 7.

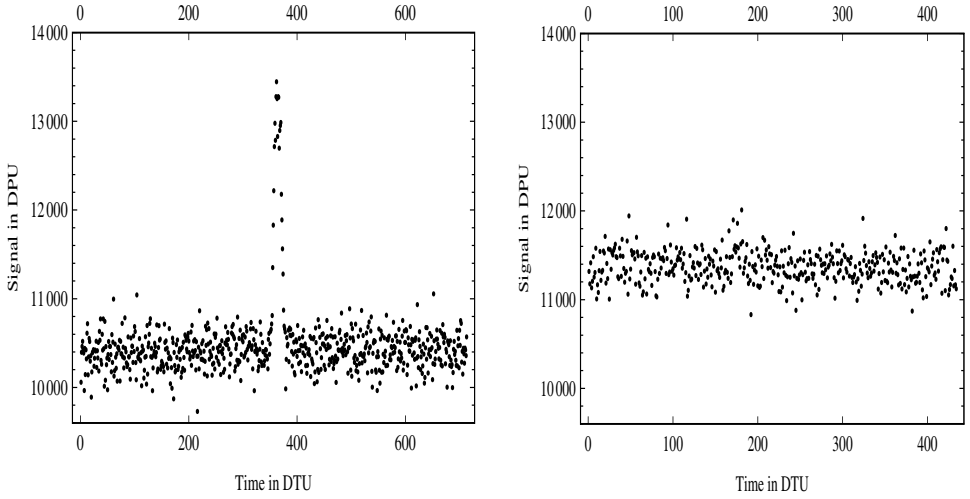

Figure 13. A high fluctuation in the star signal in a star sense of the star β-Cnc, GOES–10, on January 10, 2006: On the left is the star–signal profile of the first look, registered on Detector 1, at UTC 22:11:10.012, with a signal of 6.79 DPU. On the right is the star–signal profile of the same star in the second look, registered on Detector 3, at UTC 22:11:25.667, with a signal 0.70 DPU.